2023-01-0272 Published 11 Apr 2023



Combustion Characteristics of Low DCN Synthetic Aviation Fuel, IPK, in a High Compression Ignition Indirect Injection Research Engine

Valentin Soloiu, Amanda Weaver, Richard Smith, Aidan Rowell, John Mcafee, and James Willis Georgia Southern University

Citation: Soloiu, V., Weaver, A., Smith, R., Rowell, A. et al., "Combustion Characteristics of Low DCN Synthetic Aviation Fuel, IPK, in a High Compression Ignition Indirect Injection Research Engine," SAE Technical Paper 2023-01-0272, 2023, doi:10.4271/2023-01-0272.

Received: 08 Nov 2022 Revised: 10 Jan 2023 Accepted: 31 Jan 2023

Abstract

he Coal-To-Liquid (CTL) synthetic aviation fuel, Iso-Paraffinic Kerosene (IPK), was studied for ignition delay, combustion delay, pressure trace, pressure rise rate, apparent heat release rate in an experimental single cylinder indirect injection (IDI) compression ignition engine and a constant volume combustion chamber (CVCC). Autoignition characteristics for neat IPK, neat Ultra-Low Sulfur Diesel (ULSD), and a blend of 50%IPK and 50% ULSD were determined in the CVCC and the effects of the autoignition quality of each fuel were determined also in an IDI engine. ULSD was found to have a Derived Cetane Number (DCN) of 47 for the batch used in this experimentation. IPK was found to have a DCN of 25.9 indicating that is has a lower

affinity for autoignition, and the blend fell between the two at 37.5. Additionally, it was found that the ignition delay for IPK in the CVCC was 5.3 ms and ULSD was 3.56 ms. This increase in ignition delay allowed the accumulation of fuel in the combustion chamber when running with IPK that resulted in detonation of the premixed air and fuel found to cause high levels of Ringing Intensity (RI) when running neat IPK indicated by the 60% increase in Peak Pressure Rise Rate (PPRR) when compared to ULSD at the same load. An emissions analysis was conducted at 7 bar Indicated Mean Effective Pressure (IMEP) for ULSD and the blend of 50% ULSD and 50% IPK. With the addition of 50% IPK by mass, there was found to be a reduction in the NO_x , CO_2 , with a slight increase in the CO in g/kWh.

Introduction

he research and development of sustainable alternative fuels provides an opportunity to relieve some of the environmental pressures due to growing demand for fossil fuels and possible resource scarcity. New sustainable, clean burning fuels have the potential to replace petroleum fuel without significant modification to current engine configurations. Alternative fuels can be produced from several bio resources and are currently used in on-road vehicles though blends greater than B50 are not approved for all vehicles. Similarly, Sustainable Aviation Fuels (SAFs) are blended with petroleum aviation fuels.

Produced using the Fischer-Tropsch process, Sustainable Aerospace Fuels (SAF) are purer fuels which potentially produce fewer harmful emissions. They are developed using feedstocks which contain a sufficient quantity of hydrocarbons such as coal, natural gas, and biomass [1]. The properties of the resulting fuel changes depending on the feedstock used to produce the fuel. When coal is used, the fuel produced is Iso-Paraffinic Kerosene (IPK). It is made primarily of branched

chain hydrocarbons and had a far lower DCN than petroleum aviation fuels. Due to the purity of Fischer-Tropsch fuels, they lack aromatics and sulfur content. These components have an influence on the fluidic properties of the fuels. Low levels of these components reduce the heat of vaporization, viscosity, and lubricity [2].

IPK has been previously investigated for combustion and emissions characteristics in an aerospace context by Soloiu et. al. in a Constant Volume Combustion Chamber (CVCC) and in a turbojet engine. It was analyzed for NVH and emissions characteristics. It was found that IPK had a significant reduction in NO, UHC, and CO emissions in addition to a reduction in NVH signature and increase in thermal efficiency [3, 4, 5, 6, 7, 8, 9]. The goal of this study is to research in detail the thermophysical and combustion properties of IPK to contribute to the fundamental understanding of this alternative fuel. IPK was compared to a baseline of ULSD as well as a by mass blend of 50% IPK and 50%ULSD both in a CVCC as an Indirect Injection (IDI) Compression Ignition (CI) research engine.

Thermophysical Properties

Several investigative procedures were performed to analyze the thermophysical properties of neat IPK and ULSD. These procedures provide results that give context to the combustion characteristics of the fuels in the CI engine as well as the CVCC. Investigations were performed to indicate the spray droplet distribution, spray pattern, and mixture formation as well as the vaporization rate and low temperature oxidation through thermogravimetric analysis and differential thermal analysis. These properties influence the physical ignition delay of the fuel [10, 11, 12, 13]. Additionally, since the fuel's chemical composition plays a key role in the thermophysical properties, emissions profile, and combustion characteristics, further analyses were performed for: heat of combustion, viscosity, and volatility. The results of these analysis will be expounded in the following chapters.

From the comparison of the thermophysical properties of neat IPK and ULSD, it is apparent that those for IPK are more favorable for combustion as they would reduce the physical ignition delay. Some of the critical thermophysical properties such as the Ignition Delay (ID), Derived Cetane Number (DCN), Lower Heating Value (LHV) and Higher Heating Value (HHV), viscosity and density at 40°C, and Combustion Delay (CD) are provided in <u>Table 1</u> as well as the percent difference between the values for IPK when compared to ULSD. The chemical composition for ULSD and IPK is provided in <u>Table 2</u>, including the paraffin and hydrocarbon distributions. The heat of combustion was determined with a Parr 1341 digital constant volume calorimeter. The

TABLE 1 Thermophysical Properties of Neat Researched Fuels

	Accuracy	ULSD	IPK	% Difference
LHV (MJ/kg)*	±0.3%	41.1	44.25	7.66
HHV (MJ/kg)*	±0.3%	45.16	48.63	7.68
DCN*	±0.3%	47	25.88	-44.94
Avg. ID (ms)*	±0.1%	3.56	5.3	48.87
Avg. CD (ms)*	±0.1%	5.15	17.2	233.98
Viscosity @ 40°C (cP)*	±1.0%	2.44	1.02	-58.19
SMD [μ m]*	±1.0%	22.36	14.96	-33.09
Density @ 40°C (g/cm³)	-	0.82	0.74	-9.75

*Determined in Georgia Southern University's Automotive Combustion Laboratory

TABLE 2 Chemical Composition for Neat ULSD and Neat IPK [16, 17]

Composition	ULSD	Sasol IPK
n-Paraffins (wt%)	25-50	2.1
Iso-paraffins (wt%)		88
Cyclo-paraffins (wt%)	20-40	9
Aromatics (wt%)	15-40	<0.5
Total sulfur (wt%)	Max 0.05	< 0.001

viscosity was evaluated using a Brookfield DV-II +Pro rotational viscometer.

Evaluated in the investigation of the thermophysical properties investigation are the chemical and physical ignition delays for ULSD and IPK. The physical ignition delay is the time from Start of Injection (SOI) to the point at which active exothermic reactions begin to take place. This is affected by the physical properties of the fuel such as volatility, viscosity, density, etc. From the point at which exothermic reactions begin to take place to the Start of Combustion (SOC) is defined as the chemical ignition delay [14]. This point which defines the separation between the physical and chemical ignition delays is referred to as the Point of Inflection (POI) [14]. The chemical ignition delay depends on the chemical composition of the fuel and encompasses the amount of time required for the completion of pre-flame reactions [15].

Low Temperature Oxidation and Thermal Stability

Based on the thermophysical properties and chemical compositions, an analysis was conducted to determine the combustion properties of IPK and ULSD. The oxidation at low temperatures was investigated using a thermogravimetric analysis (TGA), and the thermal stability was examined using a differential thermal analysis (DTA). This was conducted using the Shimadzu DTG-60 and was conducted using a small sample for the research fuel weighing approximately 10 mg. The furnace was heated from 20°C to 600°C in 20°C increments per minute with a constant air flow at the rate of 15 mL/min to continually purge the furnace of fumes developed from the oxidation of the fuel. To ensure accurate results, a baseline material of inert alumina powder was used in tandem with the research fuel due to the negligible loss in mass as the chamber is heated and cooled.

The TGA is used to measure the vaporization rate of the research fuel with respect to percentage reduction in the mass as a function of the temperature. Based on the TGA in Figure 1, IPK is shown to have a much higher rate of vaporization than ULSD. This high rate of vaporization indicates IPK has a much higher volatility than ULSD. Fuels with high volatility form a more homogeneous fuel-air mixture in less time and at lower temperatures than low volatility fuels [18, 19]. The experimental IDI engine used in this investigation was chosen for its dual combustion chamber configuration as well as its high turbulence, compression ratio, chamber pressure, and chamber temperature.

The TGA of IPK and ULSD can be more exactly seen in <u>Table 3</u>, where the temperatures shown are recorded where the fuel samples reach 10%, 50%, and 90% of the fuels initial mass is vaporized. These are denoted as TA10, TA50, TA90 respectively. At 10% of the initial mass vaporized, ULSD and IPK are much closer in value (100 and 71.76 respectively) than once the temperatures are recorded at 90% initial mass vaporized (230.2 and 131.2 respectively).

The DTA is used to quantify the absorption and release of energy as a function of temperature. These endothermic processes are represented by a negative slope and exothermic reactions are represented by a positive slope. The magnitude

COMBUSTION CHARACTERISTICS OF LOW DCN SYNTHETIC AVIATION FUEL, IPK



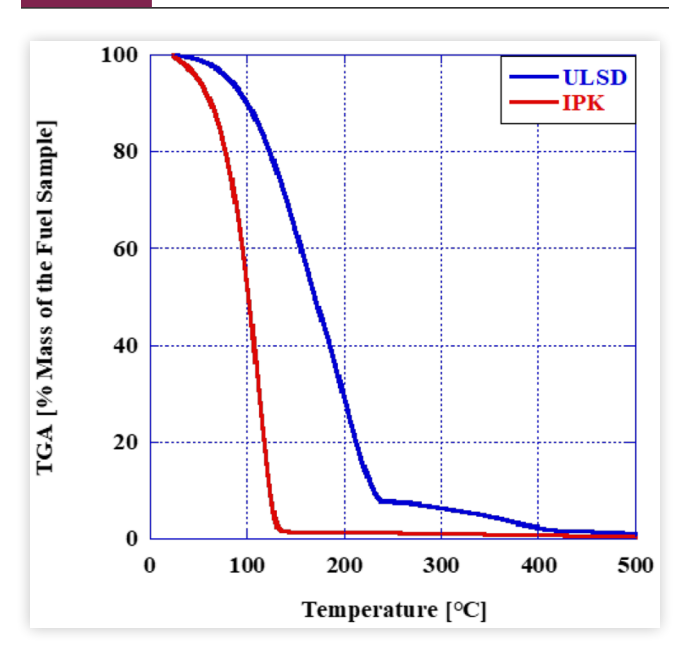


TABLE 3 Thermogravimetric Analysis (TGA)

	ULSD	IPK
TA (10) °C	100.0	71.7
TA (50) °C	170.0	108.1
TA (90) °C	230.2	131.2

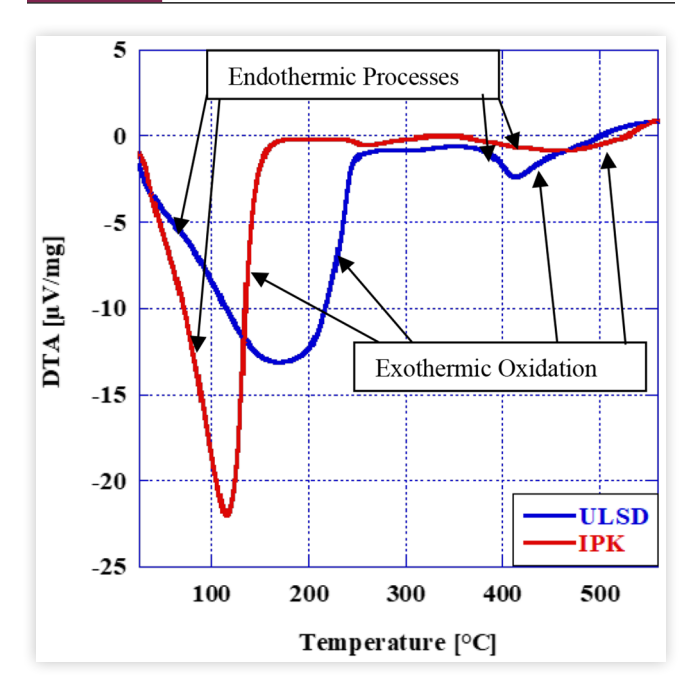
of the slope represented the rate of the energy absorption and release. Figure 2 below shows the DTA for IPK and ULSD.

The DTA results show the much higher rate of energy release and absorption for IPK at much lower temperatures as compared to ULSD. At mid temperature ranges (between 150°C and 350°), IPK is mostly stable (indicating a lack of energy release and absorption) and at the higher temperatures (350°+), there is a slight exothermic reaction. For ULSD, there is a much slower rate of energy release and absorption reaching a negative peak at 170°C. Mid temperature ranges (250°C to 380°C) depict a stable condition, and at temperatures above 400°C, there is a much smaller endothermic reaction followed by a steady exothermic reaction. The differences in the DTA for IPK and ULSD can be attributed to the more prevalent and heavier hydrocarbons in ULSD, as well as the higher volatility of IPK. The composition of unsaturated, branch chain iso-paraffins in IPK also contribute to these higher rates of energy release and absorption.

Spray Atomization, Droplet Distribution, and Mixture Formation Investigations with a Mie Scattering He-Ne Laser Apparatus

The analysis for droplet distribution, spray atomization, and mixture formation for neat IPK, neat ULSD, and 50% IPK 50% ULSD was conducted using a Malvern Spraytec He-Ne

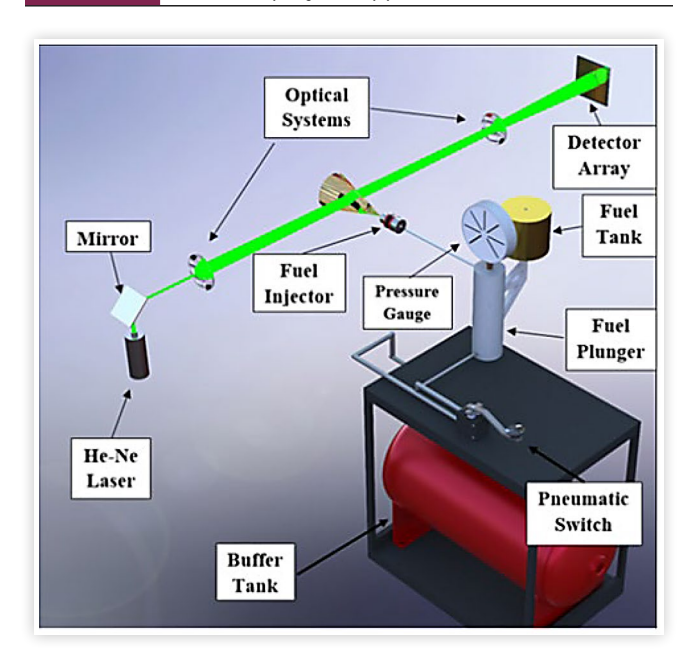
FIGURE 2 TGA of Neat ULSD and Neat IPK



laser. This apparatus (shown in <u>Figure 3</u>) uses a laser beam and light detectors to analyze the spray characteristics when an injection is triggered. The injection pressure of the fuels was 180 bar from a witness injector, and the injector was placed 100mm away from the laser beam. This distance was chosen was chosen for measurement as this is within the working distance of the lenses to avoid optical vignetting. The focal length of the laser is 300mm away from the lens. At a distance of 150mm, droplets larger than $0.5~\mu m$.

Twenty-eight light detectors reported data at 10 kHz from 0.1 ms before trigger to 5 ms after trigger. Mie Scattering and Fraunhofer diffraction theory was used to interpret the data

FIGURE 3 Malvern Spraytec Apparatus



by determining the Sauter Mean Diameter (SMD) of the spray droplets as a result of the diffraction of the laser.

The SMD is determined with two equations which describe the scattering of unpolarized light by a spherical droplet (<u>Equation 1</u>) [20].

$$I(\theta) = \frac{I_0}{2k^2a^2} \left(\left[S_1(\theta) \right]^2 + \left[S_2(\theta) \right]^2 \right) \tag{1}$$

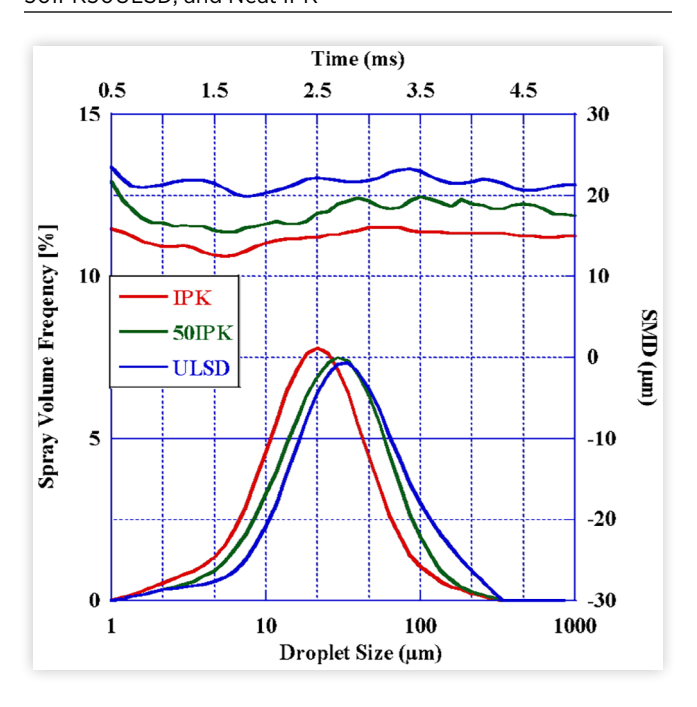
In Equation 1, $I(\theta)$ represents the light intensity after scattering occurs as a function of the angle θ , the angle the light hits the droplet relative to where it was detected. $S_1(\theta)$ and $S_2(\theta)$ represent complex, dimensionless functions which account for the change in amplitude of the parallel and perpendicular polarized light. Additionally, a is the measured distance between the detector and the light source, k is the wavenumber in $2\pi/\lambda$, and I_0 describes the initial intensity of the beam.

For a more practical application of the theory of light scattering by droplets in a variety of mixtures and shapes, the Fraunhofer diffraction theory is well suited because it does not rely on the droplet's optical properties (Equation 2) [20]. The terminology for this equation is the same as above, with the addition of the dimensionless size parameter $\alpha = \pi x/\lambda$ where x is the particle size.

$$I(\theta) = \frac{I_0}{2k^2a^2} \alpha^4 \left(\frac{J_I(\alpha \sin(\theta))}{\alpha \sin \theta} \right)$$
 (2)

For the three fuels presented herein, the averages for both SMD and droplet distribution were taken to provide an accurate representation of the spray profile of the fuels. These results are presented in <u>Figure 4</u>. The lowest droplet size over

FIGURE 4 Spray Development for Neat ULSD, 50IPK50ULSD, and Neat IPK



the control volume in the spray was found to belong to IPK. This is due to ULSD possessing a higher viscosity when compared to IPK, resulting in the droplet distribution being skewed to a higher droplet diameter. The blended fuel 50% IPK 50% ULSD by mass had an SMD which fell between the neat fuels.

CVCC Experimental Methods

The constant volume combustion chamber experiments were conducted using a Petroleum Analysis Company (PAC) CID 510. This instrument permitted an investigation into the pressure trace, heat release, ignition delay, combustion delay, low temperature heat release, and high temperature heat release for each researched fuel. This apparatus conventionally operates by first, cycling through 5 chamber conditioning periods, where fuel is injected, combusts, and exhausts. Following this chamber conditioning, measurements are taken for 15 combustion cycles. The pressure data for each cycle is recorded and is averaged. These test cycles are representative of ASTM standard D7667-14a, which can be seen in Table 4.

The schematic seen in Figure 5 details the physical components of the PAC CID 510. The cross-sectional view shows the common rail fuel injection system (denoted as 1) and the 6 orifice Bosch high pressure fuel injectors (denoted as 2). The combustion occurs in the uniformly heated, constant volume, and pressure controller combustion chamber which can be seen labeled as 2 in the external model. The component labeled 3 is the pressure sensor that measures the increase in pressure during combustion. Finally, the fuel line pressure is measured with a pressure sensor, seen as component 4.

Combustion Pressure and Ringing in CVCC

The pressure trace for each of the researched fuels were recorded, averaged, and compiled together in Figure 6. These results display the extended duration of combustion for IPK as opposed to ULSD. The combustion duration for IPK was found to be approximately 19.32 ms, while ULSD was a much shorter time of 3.64 ms. This difference resulted in the 50IPK/50ULSD blend to fall between the two neat fuels, with a combustion duration of 8.36 ms. From this data, it can be inferred that the blending of ULSD with IPK increases the combustion duration of the fuel and has the potential of reducing fuel consumption and emissions [21, 22].

Another aspect of interest in the pressure trace was the pressure ringing effect of ULSD. <u>Figure 7</u> is version of the pressure trace graph at the peaks and uses a logarithmic scale on the x-axis for easier analysis. It can be seen in <u>Figure 7</u> that there is a clear oscillation of the pressure when testing the

TABLE 4 CVCC Parameters based on ASTM D7668-14.a

Wall	Fuel Injection	Coolant	Injection	Chamber
Temp.	Pressure	Temp.	Pulse Width	Pressure
595.5 °C	1000 bar	50 °C	2.5 ms	20 bar

COMBUSTION CHARACTERISTICS OF LOW DCN SYNTHETIC AVIATION FUEL, IPK

FIGURE 5 PAC CID 510 Constant Volume Combustion Chamber

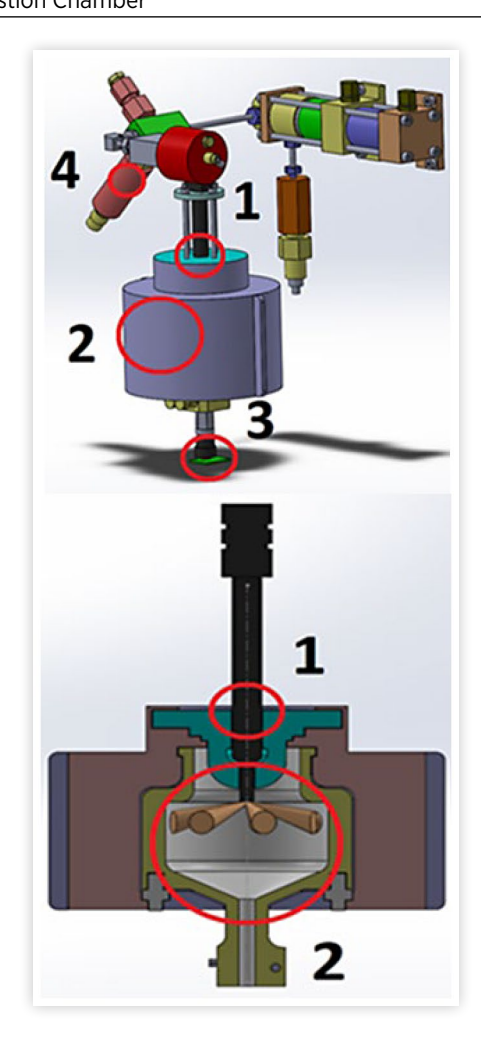


FIGURE 6 Pressure Traces for Neat ULSD, 50ULSD50IPK, and Neat IPK

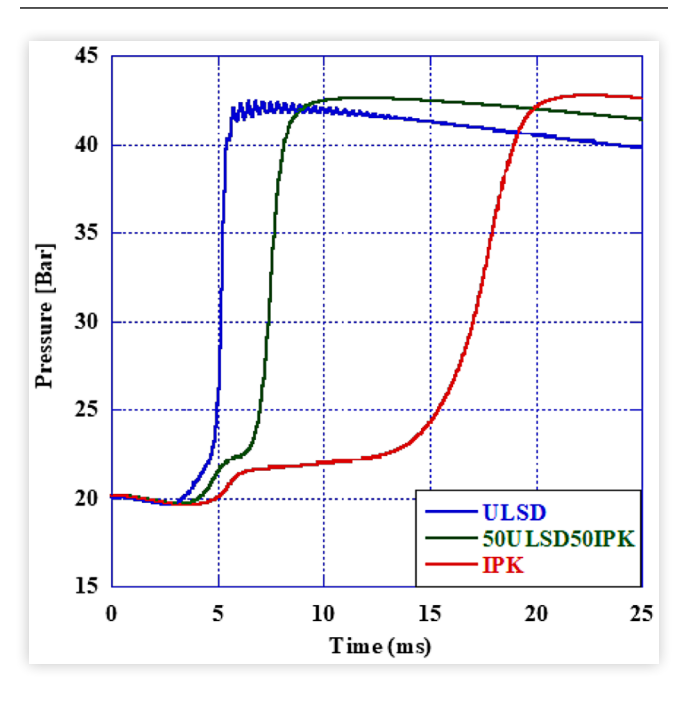
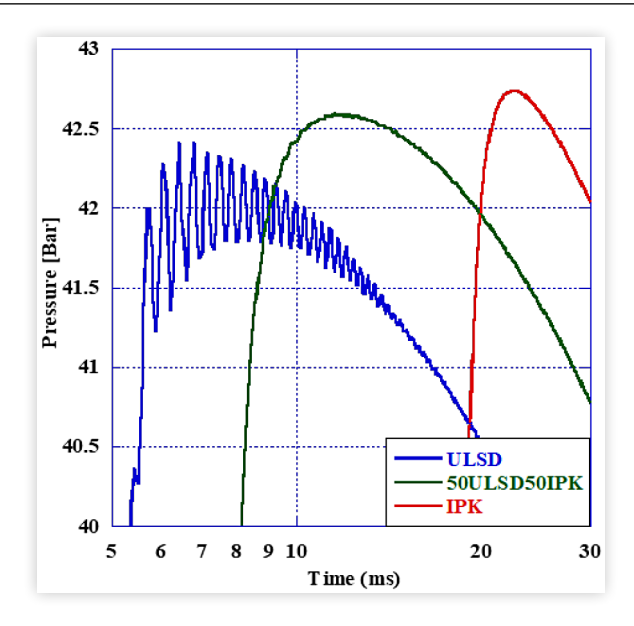


FIGURE 7 Peak Pressures for the Researched Fuels on a Logarithmic Scale



ULSD. By adding an amount of 50% by mass IPK to the ULSD fuel, the results show practically a complete reduction in ringing of the fuel in the chamber. This reduction in ringing is most likely caused by IPK's higher ignition delay, combustion delay, and lower DCN. In the CVCC, IPK has the longest Apparent Heat Release rate as seen Figure 8 further contributing to the reduction in peak pressure oscillations. This is an indication of IPK's chemical ignition delay due to its high concentration of highly branched alkanes and low DCN [23, 24].

The peak pressure and time to peak pressure can be seen below in <u>Table 5</u>. This time is measured from the time of

FIGURE 8 AHRR for Neat ULSD, 50ULSD50IPK, and Neat IPK

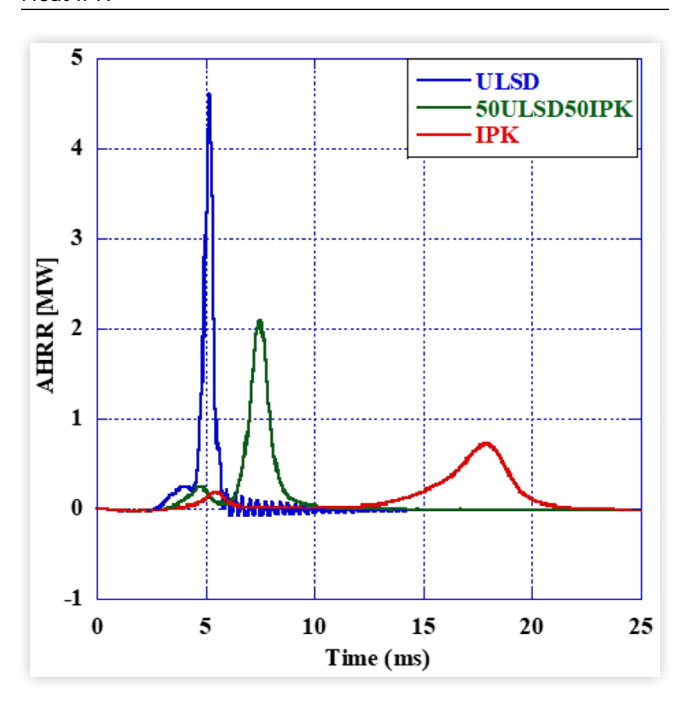


TABLE 5 Peak Pressure and Timing

Researched Fuel	ULSD	50IPK50ULSD	IPK
Time (ms)	6.44	11.56	22.6
Peak Pressure (bar)	42.41	42.58	42.73

injection to the time at which pressure is maximized. This table clearly shows the higher peak pressure and longer ignition delay and combustion delay of IPK as compared to the other researched fuels.

Apparent Heat Release Rate (AHRR) and Low-Temperature Heat Release (LTHR) Regions in CVCC

The apparent heat release rate is used to differentiate between different regions of combustion and can be calculated from the pressure during combustion. With the CVCC being modeled as a closed loop system where heat transfer is neglected and the wall temperature is constantly 595.5°C, the time of the combustion occurs at 0.04 ms after injection timing and the global specific heat ratio is assumed to be equivalent across all 15 combustion cycles [25, 26, 27, 28, 29, 30]. The equation for this can be found below in Equation 3 with a gamma value of 1.4.

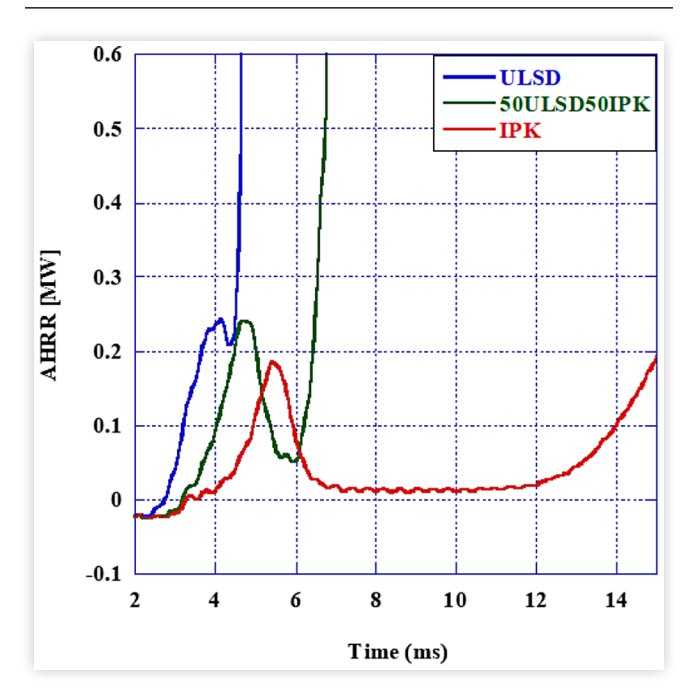
$$dQ/dt = \frac{1}{\gamma - 1}V\frac{dP}{dt} \tag{3}$$

The AHRR as a function of time can be seen in Figure 8. By comparing each fuel's peak heat release rate, it can be inferred that ULSD releases heat at a higher rate than IPK. Despite the thermophysical properties of IPK being more ideal for combustion, high volatility and smaller spray atomization when compared to ULSD, it has a much slower period of combustion. IPK reached peak AHRR at around 17 ms whereas ULSD reached its peak at 5 ms. The addition of IPK to the ULSD reduces the rate of heat release, and the absence of ULSD in IPK results in a much lower heat release rate.

Another important aspect of the apparent heat release rate is the low temperature heat release region. Figure 9 shows the AHRR vs time graph expanded around the LTHR region to better examine this area. This region it known as the point in combustion where the hydrocarbon bonds are broken, resulting in low-luminosity blue flames known as cool flames. The formation of heavy peroxides, predominantly consisting of ketohydroperoxides, results in a decrease in the AHRR, forming what is known as the negative temperature coefficient region. By expanding the duration of this area, lower emissions can be achieved [27].

<u>Figure 9</u> shows the Low Temperature Heat Release (LTHR) and Negative Temperature Coefficient Region (NTCR) of each of the researched fuels. IPK clearly shows a much more expanded NTCR as compared to ULSD. By creating a 50IPK/50ULSD fuel blend, it can clearly be inferred that the NTCR is increased in the amount of time it persists. The thermophysical properties of ULSD indicate the fuel will

FIGURE 9 LTHR for Neat ULSD, 50ULSD50IPK, and Neat IPK



have less desirable autoignition characteristics than IPK. However, the CVCC investigation of the combustion characteristics of IPK and ULSD show ULSD has more favorable autoignition characteristics based on the extended ID and CD of IPK. These LTHR and NTC regions have been linked to the emissions characteristics of the fuel's burn [28].

Combustion Analysis in an IDI Experimental Engine

For the dynamic combustion analysis, an IDI research engine was instrumented to perform an investigation into the performance and emissions of neat IPK and a by mass blend of 50% ULSD and 50% IPK with a baseline of neat ULSD at 5, 6, and 7 bar IMEP and 2400 rpm. The engine instrumentation can be seen in Figure 10. The engine utilizes a triple vortex swirl

FIGURE 10 IDI Research Engine Configuration [29]

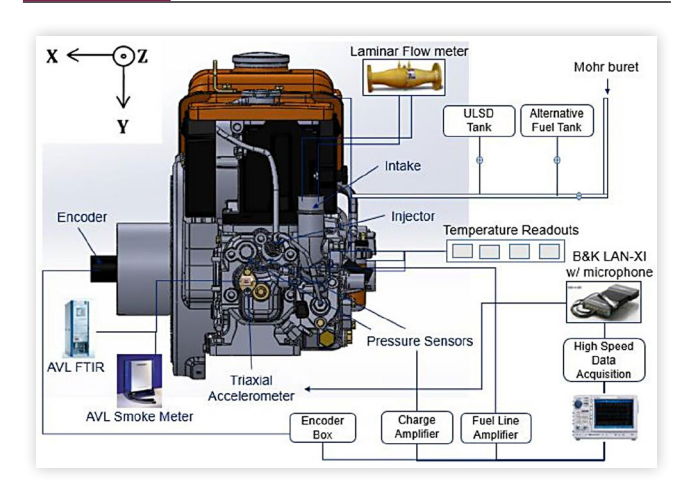


FIGURE 11 Triple Vortex High Turbulence Separate Combustion Chamber [29]

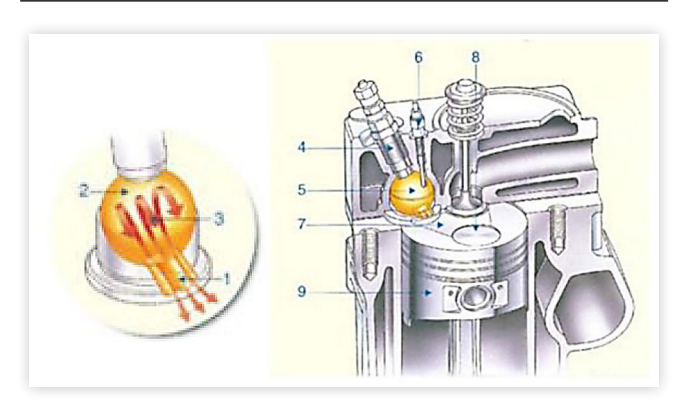
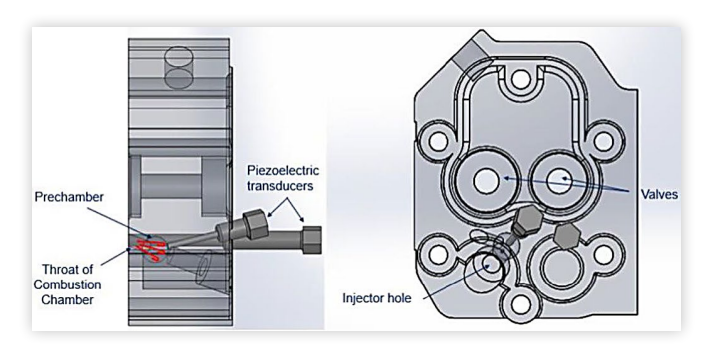


FIGURE 12 Cylinder Head Instrumentation with Pressure Sensor using Glow Plug Adaptor (Kistler type 6053 CC)



chamber into which fuel is injected to increase fuel-air mixing without increasing injection pressure. A cut through of the pre-chamber can be seen in <u>Figure 11</u>.

The engine is liquid cooled, naturally aspirated and mounted on a hydraulic dynamometer. Injection pressure is 150 bar through a Pintaux type 1x0.200mm nozzle. All associated engine parameters are listed in <u>Table 6</u>. Combustion chamber pressure was measured for both the swirl chamber and the main chamber. Main chamber pressure was measured using Kistler type 6053 CC and pre chamber pressure as measured using a Kistler type 6056 A. TDC and CAD were determined using an OMRON E6C2 optical rotary encoder

TABLE 6 Physical Specifications for the Research IDI Engine

Parameter	Value
Emissions Regulation	Tier 4
Displaced volume	0.35 L
Stroke	70 mm
Bore	77 mm
Connecting Rod Length	111 mm
Compression ratio	23.5:1
Injection Nozzle	1 Orifice x 0.20 mm
Injection Pressure	150 bar
Number of Cylinders	1
Engine Effective Power	5.2 kW@ 3000 rpm
Engine Effective Torque	18 Nm @ 2400 rpm

with a capture rate of 2000 pulses per revolution. Data was captured using a Yokogawa DL850 high speed data acquisition system.

During the high turbulence combustion, the fuel impingement in the high vortex separate combustion chamber causes a short ignition delay and multi-fuel capability [27, 28, 29, 30, 31, 32]. The air mixture formation of the fuel and the air has a significant impact on the peak heat release while the spray break and vaporization properties are primarily dependent on the turbulence in the pre-chamber. The ignition delay also plays a significant role in the peak heat release during combustion.

Due to the high turbulence, temperature, pressure, and compression ratio in the triple vortex combustion chamber, the premixed and diffusion phases of combustion are compounded [30]. The two phases of heat release seen in Apparent Heat Release Rate (AHRR) shown in Figure 20 are due to the fluidic interaction between the two combustion chambers. With this high swirl and high turbulence configuration, there was not observed to be a significant level of diffusion burn. The two peaks which can be seen in the AHRR curve are associated with combustion in the pre-chamber and the main chamber. The P-v diagram and main chamber pressure trace and displayed Figures 13 and 14 with peak pressures shown in Table 7 for each of the researched fuels.

IPK has ideal thermophysical properties for short physical ignition delay which include its small droplet size, high volatility, low density, and high heat of combustion, however, the chemical ignition delay is overwhelmingly longer indicated by the low DCN in conjunction with these properties cause significant levels of detonation in the engine. The ID and CD observed in the CVCC indicate a delay in combustion in the CI engine. IPK was found to have a very long delay in ignition at 7 bar IMEP.

FIGURE 13 P-V Diagram for Neat ULSD, 50ULSD50IPK, and Neat IPK at 7 bar IMEP.

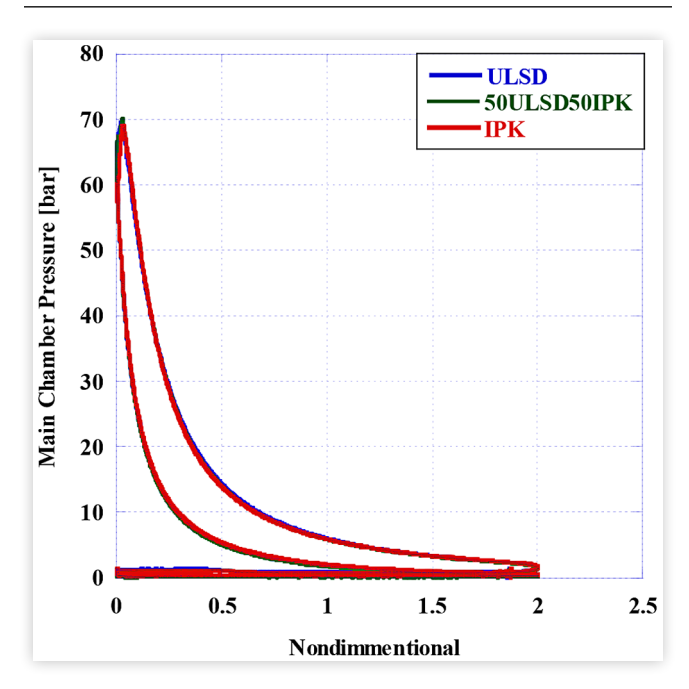


FIGURE 14 Combustion Pressure for Neat ULSD, 50ULSD50IPK, and Neat IPK.at 7 bar IMEP

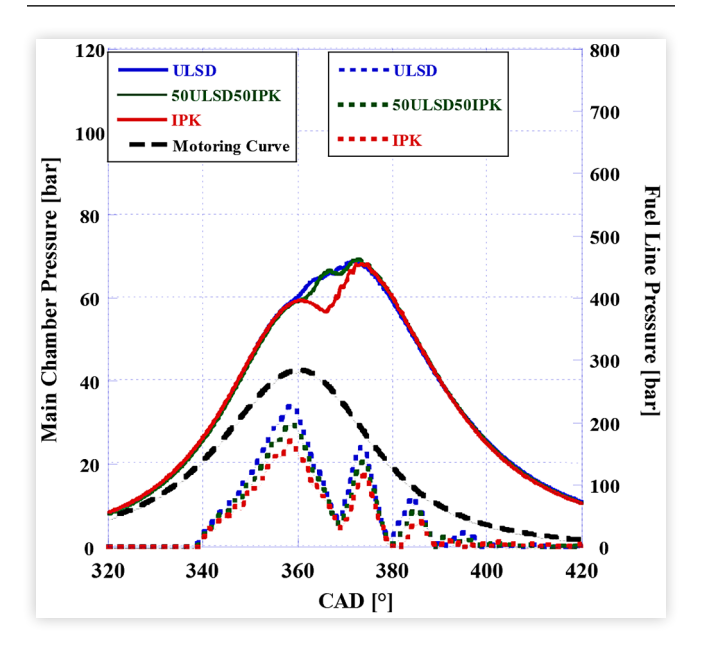


TABLE 7 Peak Pressure at 7 bar IMEP

Researched Fuel	Peak Pressure bar/CAD
ULSD	69.5/371
50ULSD50IPK	68.9/372.40
IPK	68.9/372.80

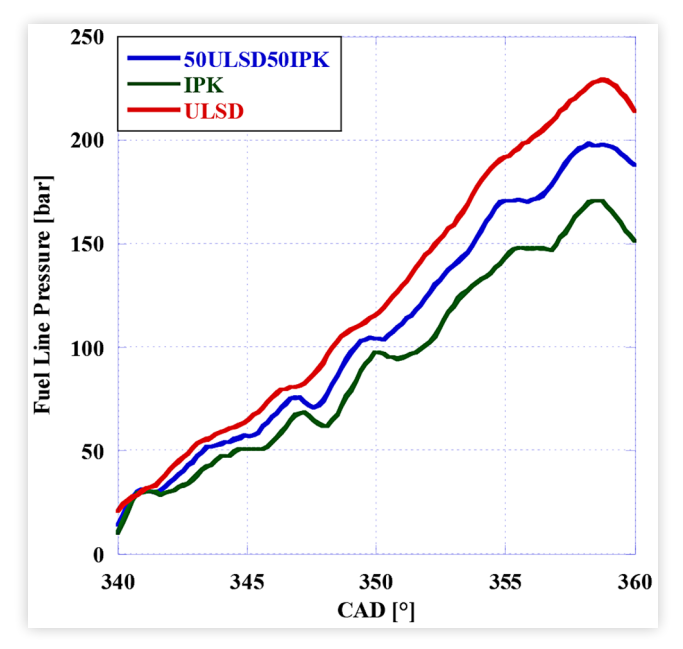
IPK's high resistance to autoignition extends the amount of time necessary for the complete mixing of the spray providing quasi homogeneous conditions. This then creates ideal conditions for rapid flame propagation and steep Pressure Rise Rate (PRR) as seen in Figure 18. Table 7 contains the peak pressures and the measured CAD for which each peak pressure occurred.

The 50ULSD/50IPK blend and neat ULSD follow a similar ignition pathway, as seen in Figure 14, IPK does not begin to combust until well after TDC. Despite this late ignition, IPK reached peak pressure at a comparable timing to that of the other two fuels. This indicates a high-pressure gradient and Apparent Heat Release Rate (AHRR) and reflects the detonation found in a later analysis in Figures 18 and 20.

From an analysis of the fuel line pressure from the graphs in Figures 14 and 15, it was found that the line pressure and the pressure necessary for injection were significantly lower for IPK when compared to the 50ULSD/50IPK blend and neat ULSD. A zoom of the fuel line pressure around injection is shown in Figure 15. In addition to the reduction in fuel line pressure for IPK, there was found to be an increase in the oscillations as pressure increases before injection. These phenomena increased linearly in magnitude with the addition of IPK, a trend which is not reflected in the combustion pressure trace. Viscosity, as is a physical property, changes linearly with the addition of more of the blended fuel [35].

This reduction in fuel line pressure is due to the low viscosity and density of IPK, but it can achieve a sufficient flow

FIGURE 15 Fuel Line Pressure at Injection for Neat ULSD, 50ULSD50IPK, and Neat IPK at 7 bar IMEP



rate for injection because of the fluid dynamic properties. This, in turn, reduces the pressure necessary which is built in the fuel line as the injector is mechanically controlled and utilizes a Pintaux type nozzle. Peak pressures history is displayed in Figure 15 and peak values are displayed in Table 8. IPK reached a peak pressure of only 170.77 bar which is lower than ULSD's peak fuel line pressure at 229.25 bar. Start of Injection (SOI) was considered to be at a line pressure of 150 bar. This put SOI for ULSD, 50ULSD50IPK, and IPK at 352.26, 353.7, and 356.94 CAD respectively.

Figure 16 and Figure 17 are the in-cylinder pressure curves for IPK at 5, 6, and 7 bar IMEP. It was observed that with the increase in the engine load because of the higher temperatures in the cylinder the ignition delay was reduced though the pressure rise rate increased as IMEP increased. For a given DCN, with increased cylinder pressure the ignition delay is shortened for IPK combustion [36, 37].

The reduction in ignition delay was found to have a nonlinear correlation to the increase in load. The change in ID was far more significant between 6 and 7 bar IMEP than between 5 and 6 bar IMEP. While there was in increase in combustion chamber pressure due to the higher load, there was a significant decrease in the ignition delay.

TABLE 8 Peak Fuel Line Pressure at 7 bar IMEP

Researched Fuel	Peak Fuel Line Pressure [bar]	Linearity (%FSO)
ULSD	229.25	≤ ± 1
50ULSD50IPK	198.07	≤ ± 1
IPK	170.77	≤ ± 1

FIGURE 16 Combustion Pressure for Neat IPK at 5, 6, and 7 bar IMEP

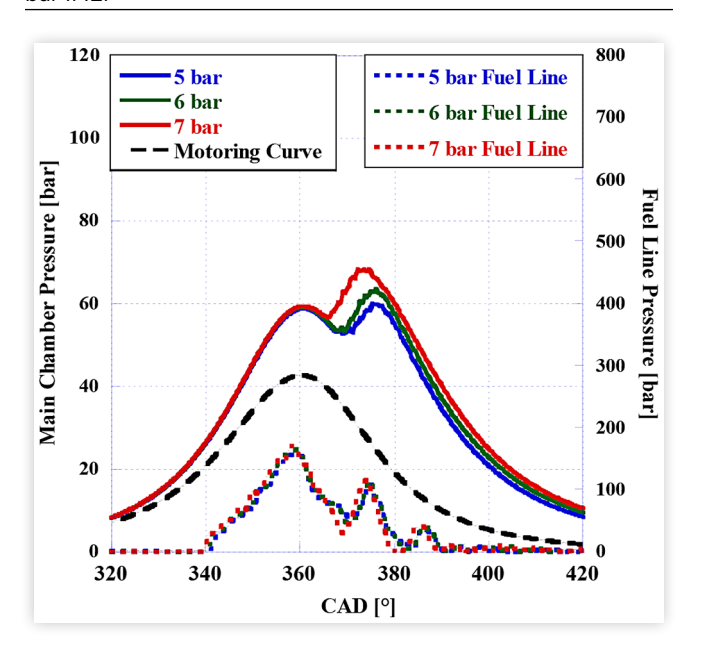


FIGURE 18 Change in Pressure vs CAD at 7 bar IMEP

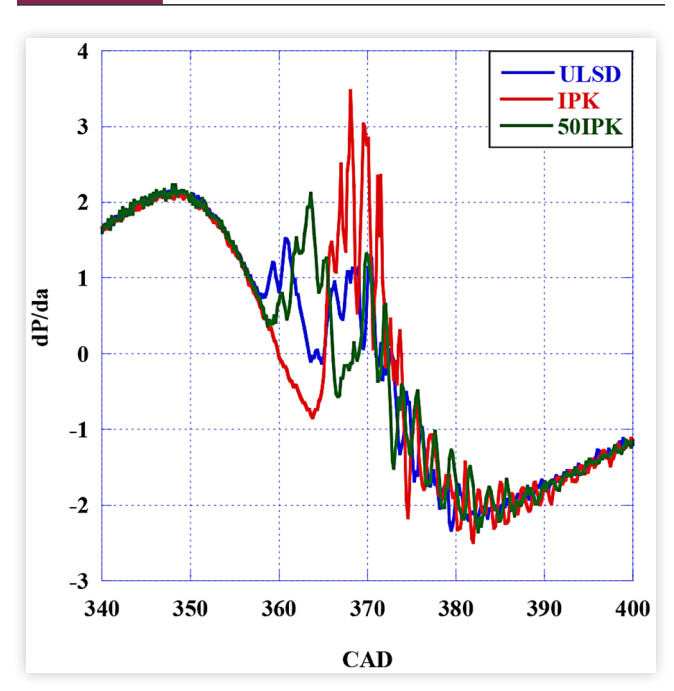


FIGURE 17 Peak Combustion Chamber Pressure for Neat IPK at 5, 6, and 7 bar IMEP

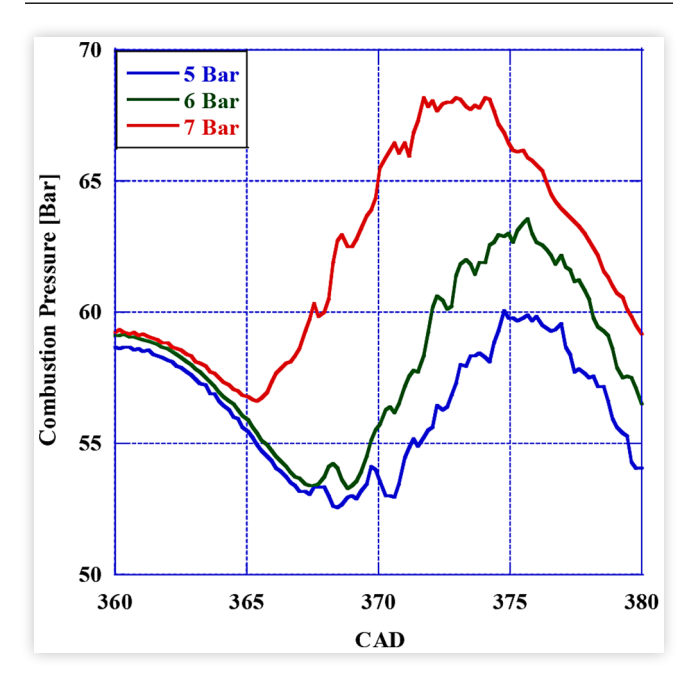
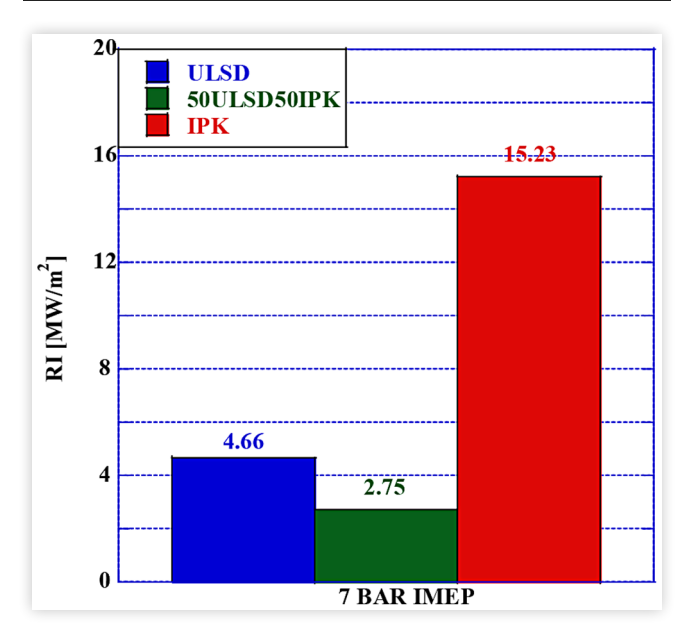


FIGURE 19 Ringing Intensity at 7 bar IMEP for Each of the Researched Fuels



Pressure Rise Rate and Ringing Intensity

An analysis of the Pressure Rise Rate (PRR) and the Ringing Intensity (RI) were performed to quantify the levels of detonation associated with the combustion of IPK. PRR and RI, shown in <u>Figures 18</u> and <u>19</u>, are calculated at 7 bar IMEP. From the graph of PRR in <u>Figure 18</u>, both ULSD and the blend of 50ULSD/50IPK began increase in PRR before TDC indicating

that the fuel begins to combust because of the high levels of swirl and turbulence as the piston is still

$$RI = \frac{\left(\beta \left(\frac{dP}{dt}\right)_{\text{max}}\right)^2}{\left(2\gamma P_{\text{max}}\right)} \sqrt{\gamma R T_{\text{max}}} \tag{4}$$

in the compression stroke. For IPK, however, the increase in pressure rise rate is delayed to nearly 365° CAD. Additionally,

TABLE 9 Peak Pressure Rise Rates (PPRR) for Each of the Researched Fuels at 7 bar IMEP

	Peak Pressure Rise	Linearity
Researched Fuel	Rate [bar/CAD]	(%FSO)
ULSD	2.16	≤ ± 0.03
50ULSD50IPK	2.23	≤ ± 0.03
IPK	3.47	≤ ± 0.03

IPK was found to have the highest Peak Pressure Rise Rate (PRR) at 3.47 bar/CAD compared to ULSD and the 50ULSD/50IPK blend at 2.16 bar/CAD and 2.23 bar/CAD respectively. All these values can be found <u>Table 9</u>. This is consistent with the high physical affinity for autoignition paired with its low chemical affinity for autoignition. The long chemical ignition delay of IPK can be attributed to its relatively low n-paraffin to iso-paraffin content [38, 39, 40]. This results in the autoignition of an unburned mixture in the end gas ahead of the propagating flame in the combustion chamber with an inverse relationship between ignition delay and compression pressure [34, 41].

For further analysis into the detonation in the combustion of IPK, Ringing Intensity (RI) was calculated for each of the researched fuels at 7 bar IMEP to correlate with the results from the PRR analysis. Equation 4 was used to calculate RI with the β value set to 0.05 as determined from literature [42]. $T_{\rm max}$ was calculated from main chamber combustion pressure and piston travel as well as using 1.4 as the value for gamma.

Results of the RI analysis are consistent with the PRR analysis with IPK having the highest level of ringing. From the graph in Figure 19, IPK had a RI three times higher than ULSD and 5.5 times higher than the 50ULSD/50IPK blend. Neat ULSD, the blend of 50ULSD/50IPK, and neat IPK were found to have an RI of 4.66, 2.75, and 15.23 respectively. Though the PPRR was higher for the 50ULSD/50IPK blend when compared to neat ULSD, the overall RI was the lowest for the 50ULSD/50IPK blend.

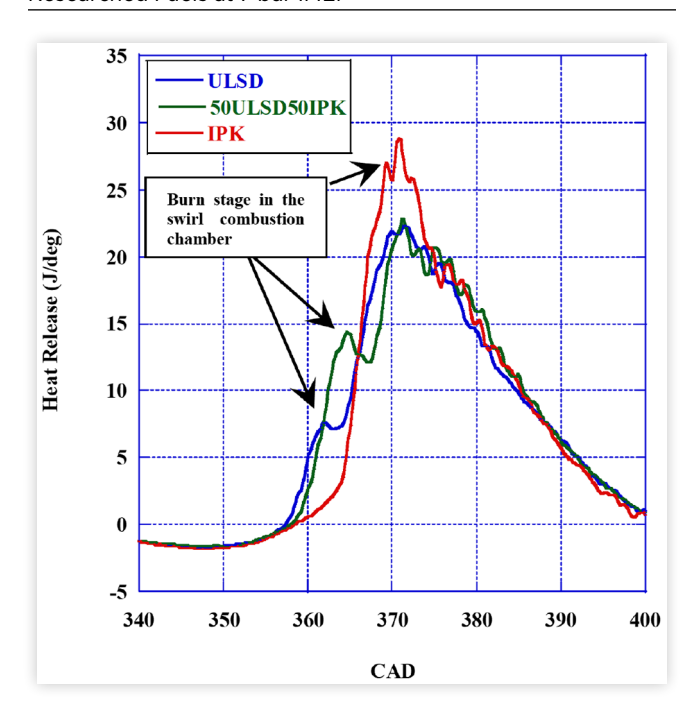
Apparent Heat Release Rate

To calculate the Apparent Heat Release Rate (AHRR) in the IDI engine, <u>Equation 5</u> is used as it works on the first principle of thermodynamics using the same value for gamma as in <u>Equations 3</u> and <u>4</u>. The system is assumed to undergo no mass transfer when bracket valves are closed, and the working fluid is treated as a homogeneous mixture of ideal gases.

$$\frac{dQ}{d\theta} = \frac{1}{(\gamma - 1)} V \frac{dP}{d\theta} + \frac{\gamma}{(\gamma - 1)} P \frac{dV}{d\theta}$$
 (5)

The resulting calculation of AHRR at 7 bar IMEP can be seen in Figure 20 for each of the researched fuels. In the AHRR for each fuel, there can be seen a dual stage combustion process denoted in the graph in Figure 20. This dual stage combustion was identified as combustion in the swirl chamber and subsequent expulsion of flames from the pre-chamber to the main chamber. These combustion stages are much more distinct for the AHRR of neat ULSD and the 50ULSD/50IPK blend. IPK, however, has a very long chemical ignition delay

FIGURE 20 Apparent Heat Release Rate for Each of the Researched Fuels at 7 bar IMEP



which allows time for the injected fuel to form a better air-fuel mixture in the separate combustion chamber which is then expelled back into the main combustion chamber. At the timing of ignition for IPK, the premixed air and fuel burn much more rapidly causing a smaller spike in the separate combustion chamber as the piston is moving to BDC and seen in Figure 20 and Figure 21.

Peak AHRR for each of the researched fuels are displayed in Table 10 in J/CAD. Neat ULSD and 50ULSD/50IPK are

FIGURE 21 Pre-Chamber Apparent Heat Release Rate for Each of the Researched Fuels

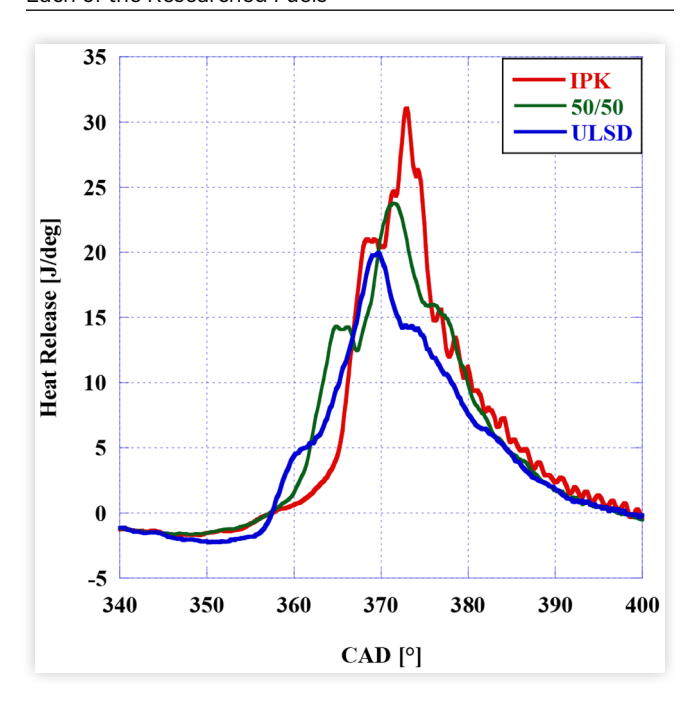


TABLE 10 Peak AHRR for Each of the Researched Fuels at 7 bar IMEP

Researched Fuel	AHRR [J/CAD]
ULSD	22.32
50ULSD50IPK	22.84
IPK	35.48

comparable at 22.32 J/CAD and 22.84 J/CAD. In alignment with the PPRR and the RI analysis, IPK was found to have the highest AHRR at 35.48 J/CAD.

The graph in Figure 22 displays the difference between the AHRRs in the swirl chamber and the main chamber. This analysis was conducted to determine the location for which the main combustion event is occurring. For this determination, the main chamber AHRR was subtracted from the swirl chamber AHRR resulting positive and negative values indicating the primary region of combustion. Positive values indicate that more heat is being released in the swirl chamber and negative values indicate that more heat is being released in the main chamber. For each of the three researched fuels, combustion begins in the swirl chamber and propagates to the main chamber with the pressure oscillating between the two chambers as combustion continues. The initial gradual increase in AHRR in the pre-chamber for each of the three fuels results from the increase in temperature of the intake air due to compression concentrating the pre-chamber. The injection event causes a dip seen in the graph of each fuel due to the drop in heat release caused by the vaporization of the fuel. This reduction in AHRR is most noticeable in the graph of IPK as IPK has the highest volatility and the lowest DCN. There is a sharp increase in the pre-chamber indicating the beginning of combustion. For ULSD and 50/50, this spike occurs right before and right after TDC respectively. IPK, in

FIGURE 22 Pre-Chamber (PC) versus Main Chamber (MC) AHRR

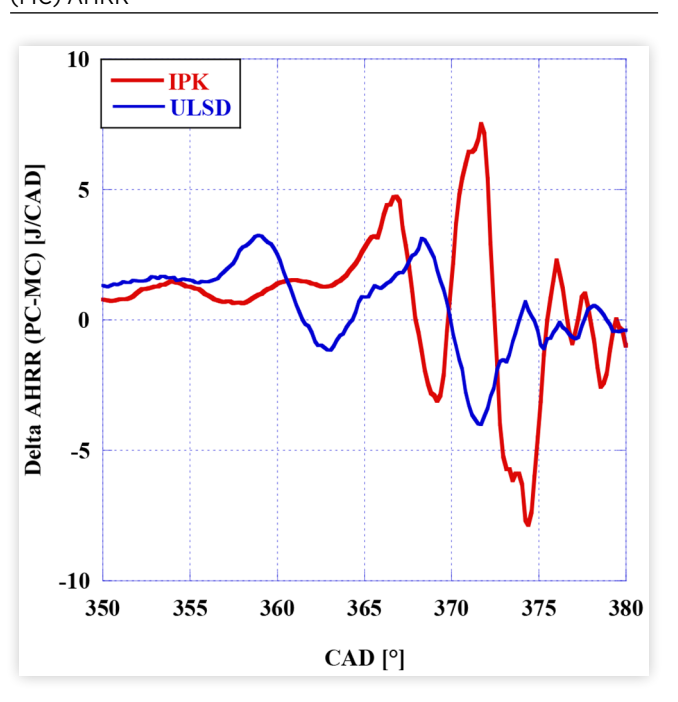
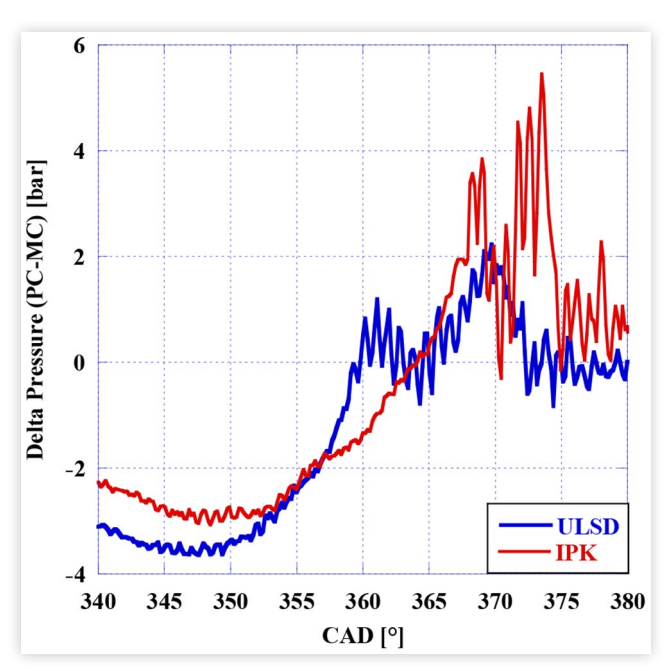


FIGURE 23 Pre-Chamber (PC) versus Main Chamber (MC)



keeping with its high resistance to autoignition, has a much delayed peak and a higher frequency and magnitude of subsequent oscillations from between the pre-chamber and the main chamber.

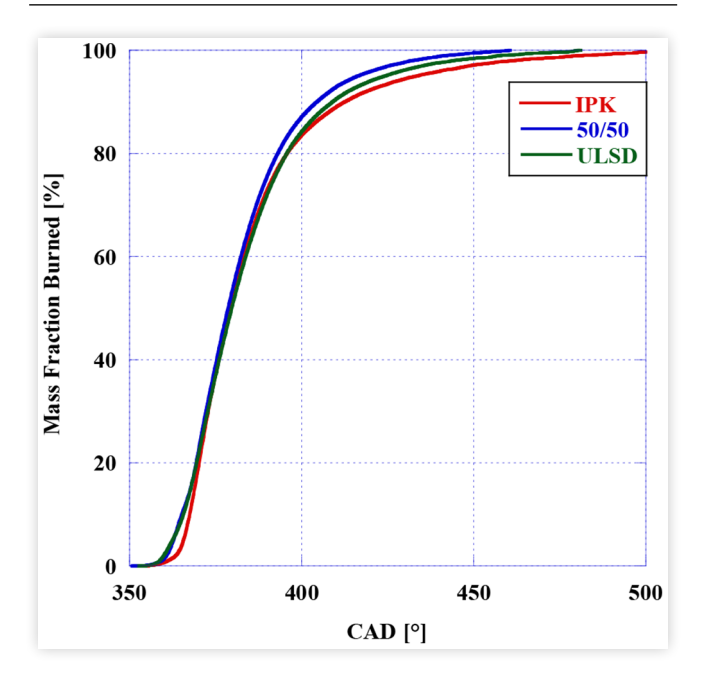
The graph in Figure 23 displays the difference between the combustion chamber pressures in the swirl chamber and the main chamber. This analysis was conducted to corroborate the location that the combustion is occurring with the delta AHRR. For this determination, the main chamber pressure was subtracted from the swirl chamber pressure resulting positive and negative values indicating the primary region of combustion. There are several ringing events which occur in the pre-chamber during the combustion of IPK. As the piston is traveling toward TDC, the pressure increases first in the main chamber. Pressure begins to increase more rapidly in the pre-chamber at around 347 CAD.

The graph in Figure 24 shows the calculation of the mass fraction burned for each of the researched fuels. This curve is calculated from the integration of the gross heat release curves from the start of injection until the heat release reaches zero. This is done as a representation of the burn rate of each of the fuels. The curve of ULSD and the 50ULSD/50IPK blend are nearly identical at the beginning of combustion but deviate as combustion continues with the 50/50 blend having the faster burn rate between the two. IPK is the slowest to begin burning and continues to combust far longer when compared to the other researched fuels.

Emissions Analysis

A study on the emissions profile was conducted for neat ULSD and 50ULSD/50IPK to determine the effect of the addition of SAF to petroleum fuel for the reducing harmful GHG emissions. Emissions species studied in this investigation were CO,

FIGURE 24 Mass Fraction Burned for Each of the Researched Fuels



UHC, NO, and CO₂. An MKS FTIR 2030 gaseous species analyzer was used to conduct the investigation.

It was found that with the addition of IPK to ULSD, there was a drop in the levels of CO, NO, and UHC. The percentages of CO_2 , however, were found to increase in concentration for 50ULSD/50IPK when compared to neat ULSD. Results for CO, UHC, and CO_2 can be found in <u>Figure 25</u> and results for NO and NO_2 can be found in <u>Figure 26</u> where the values for NO_2 are shown in ppm as they are very small when compared to the values for NO.

The drop in NO concentration observed with the combustion of 50ULSD50IPK can be attributed to the late combustion phasing [43]. This late combustion phasing caused a reduction in peak temperature and pressure with the addition of IPK to

FIGURE 25 CO, UHC, and %CO₂ for ULSD and 50ULSD50IPK at 7 bar IMEP

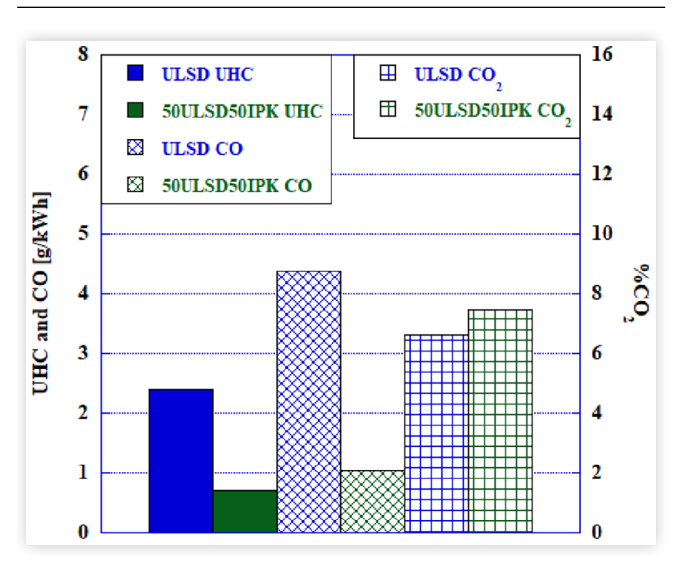
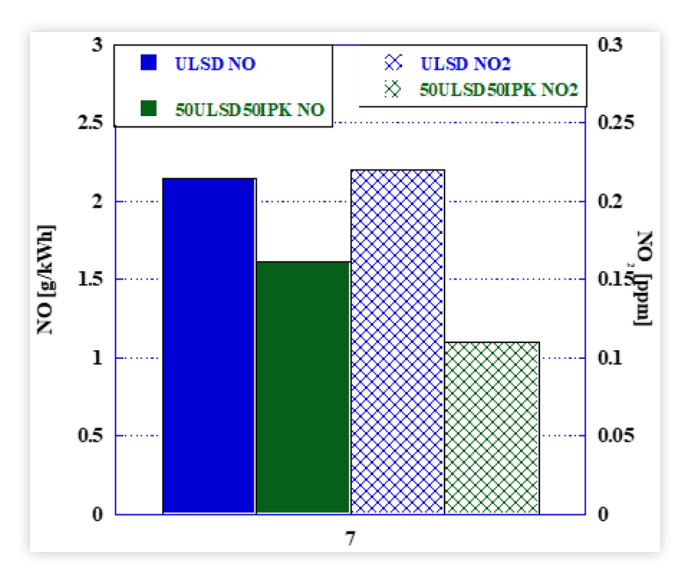


FIGURE 26 NO and NO₂ Emissions for ULSD and 50ULSD50IPK at 7 bar IMEP



ULSD [$\underline{44}$]. The increase in CO_2 and the reduction in UHC and CO indicate that with the addition of IPK to ULSD, the blended fuel undergoes more complete combustion.

Summary/Conclusions

A Fischer-Tropsch CTL SAF, Iso-Paraffinic Kerosene (IPK) was investigated to determine its thermophysical properties as well as its ignition delay, combustion delay, pressure trace, pressure rise rate, apparent heat release rate in an experimental single cylinder indirect injection (IDI) compression ignition engine and a constant volume combustion chamber (CVCC). IPK was compared to ULSD along with a mass blend of 50% ULSD and 50% IPK. In an experimental IDI engine, combustion pressure, AHRR, and PRR were determined at 5, 6, and 7 bar IMEP.

The analysis of the thermophysical properties of IPK indicated that it has a short physical ignition delay. This result comes from the analysis of the spray structure, mixture formation, droplet distribution, low temperature oxidation characteristics, viscosity, and density. IPK was found to have a combination of favorable properties for a short physical ignition delay including a high volatility, small spray droplet distribution, and low viscosity and density when compared to ULSD. The CVCC investigation for IPK and ULSD found that the chemical ignition delay for IPK is substantially longer than that of ULSD resulting in an ID of 5.3 ms compared to ULSD at 3.56 ms. This can be attributed to its relatively low n-paraffin to iso-paraffin content and high concentration of highly branched alkanes. These compound resist auto ignition and extend the ignition delay of combustion.

Experiments in the IDI engine determined that at all loads IPK exhibited high detonation levels indicated by the 60% increase in PPRR and RI when compared to ULSD. It was found that the extended chemical ignition delay allows more time for the injected fuel to accumulate in the

combustion chamber form an air-fuel mixture more favorable for combustion. This results in a large PPRR inducing pressure oscillations of high intensity and frequency between the combustion chambers.

Because of the significant levels of engine knock for IPK, a by mass blend of 50% IPK and 50% ULSD was used to study the emissions output. It was found that the blend saw a significant reduction in NO, UHC, and CO emissions at 7 bar IMEP with an increase in the $\rm CO_2$.

References

- Santos, R.G. and Alencar, A.C., "Biomass-Derived Syngas Production via Gasification Process and Its Catalytic Conversion into Fuels by Fischer Tropsch Synthesis: A Review," *International Journal of Hydrogen Energy* 45, no. 36 (2020): 18114-18132, https://doi.org/10.1016/j.ijhydene.2019.07.133.
- Lee, J. and Bae, C., "Application of JP-8 in a Heavy-Duty Diesel Engine," Fuel 90, no. 5 (2011): 1762-1770, https://doi.org/10.1016/j.fuel.2011.01.032.
- Soloiu, V., Wiley, J.T., Gaubert, R., Mothershed, D. et al., "Fischer-Tropsch Coal-to-Liquid Fuel Negative Temperature Coefficient Region (NTC) and Low-Temperature Heat Release (LTHR) in a Constant Volume Combustion Chamber (CVCC)," *Energy* 198 (2020): 117288, https://doi.org/10.1016/j.energy.2020.117288.
- Atkinson, C.M., Thompson, G.J., Traver, M.L., and Clark, N., "In-Cylinder Combustion Pressure Characteristics of Fischer-Tropsch and Conventional Diesel Fuels in a Heavy-Duty CI Engine," SAE Technical Paper <u>1999-01-1472</u> (1999), <u>https://doi.org/10.4271/1999-01-1472</u>.
- Jiao, Y., Liu, R., Zhang, Z., Yang, C. et al., "Comparison of Combustion and Emission Characteristics of a Diesel Engine Fueled with Diesel and Methanol-Fischer-Tropsch Diesel-Biodiesel-Diesel Blends at Various Altitudes," *Fuel* 243 (2019): 52-59, https://doi.org/10.1016/j.fuel.2019.01.107.
- Jürgens, S., Oßwald, P., Selinsek, M., Piermartini, P. et al., "Assessment of Combustion Properties of Non-Hydroprocessed Fischer-Tropsch Fuels for Aviation," Fuel Processing Technology 193 (2019): 232-243, https://doi. org/10.1016/j.fuproc.2019.05.015.
- Gill, S.S., Tsolakis, A., Dearn, K.D., and Rodríguez-Fernández, J., "Combustion Characteristics and Emissions of Fischer–Tropsch Diesel Fuels in IC Engines," *Progress in Energy and Combustion Science* 37, no. 4 (2011): 503-523, https://doi.org/10.1016/j.pecs.2010.09.001.
- 8. Wang, H. and Oehlschlaeger, M.A., "Autoignition Studies of Conventional and Fischer–Tropsch Jet Fuels," *Fuel* 98 (2012): 249-258, https://doi.org/10.1016/j.fuel.2012.03.041.
- Soloiu, V., Phillips, C.J., Carapia, C., Knowles, A. et al., "Exploratory Investigation of Combustion and NVH Signature of a Drone Jet Engine Fueled with IPK," in AIAA Scitech 2021 Forum, 2021, https://doi.org/10.2514/6.2021-1347.
- Jing, W., Roberts, W.L., and Fang, T., "Spray Combustion of Jet-A and Diesel Fuels in a Constant Volume Combustion

- Chamber," *Energy Conversion and Management* 89 (2015): 525-540, https://doi.org/10.1016/j.enconman.2014.10.010.
- Zeng, W., Sjöberg, M., Reuss, D.L., and Zongjie, H., "High-Speed PIV, Spray, Combustion Luminosity, and Infrared Fuel-Vapor Imaging for Probing Tumble-Flow-Induced Asymmetry of Gasoline Distribution in a Spray-Guided Stratified-Charge Disi Engine," *Proceedings of the Combustion Institute* 36, no. 3 (2017): 3459-3466, https://doi.org/10.1016/j.proci.2016.08.047.
- 12. Manigandan, S., Gunasekar, P., Poorchilamban, S., Nithya, S. et al., "Effect of Addition of Hydrogen and TIO2 in Gasoline Engine in Various Exhaust Gas Recirculation Ratio," *International Journal of Hydrogen Energy* 44, no. 21 (2019): 11205-11218, https://doi.org/10.1016/j.ijhydene.2019.02.179.
- 13. Tess, M., Kurman, M., and Kweon, C.-B., "Spray Characterization and Ignition Delay Measurements of JP-8 and IPK in a Constant-Pressure Flow Chamber," *SAE Int. J. Engines* 9, no. 2 (2016): 899-909, https://doi.org/10.4271/2016-01-0736.
- Zheng, Z., Badawy, T., Henein, N., Sattler, E. et al., "Effect of Cetane Improver on Autoignition Characteristics of Low Cetane Sasol IPK Using Ignition Quality Tester (IQT)," in Internal Combustion Engine Division Fall Technical Conference, 2013, https://doi.org/10.1115/icef2013-19061.
- 15. Ryan, T.W., "Correlation of Physical and Chemical Ignition Delay to Cetane Number," SAE Technical Paper <u>852103</u> (1985), https://doi.org/10.4271/852103.
- Farrell, J.T., Cernansky, N.P., Dryer, F.L., Law, C.K. et al.,
 "Development of an Experimental Database and Kinetic Models for Surrogate Diesel Fuels," SAE Technical Paper 2007-01-0201 (2007), https://doi.org/10.4271/2007-01-0201.
- 17. Zhang, C., Hui, X., Lin, Y., and Sung, C.-J., "Recent Development in Studies of Alternative Jet Fuel Combustion: Progress, Challenges, and Opportunities," *Renewable and Sustainable Energy Reviews* 54 (2016): 120-138, https://doi.org/10.1016/j.rser.2015.09.056.
- 18. Yousufuddin, S., "Effect of Combustion Duration on the Operating and Performance Characteristics of a Hydrogen-Ethanol Dual Fueled Engine: An Experimental Analysis," *International Journal of Advances on Automotive and Technology* (2016), https://doi.org/10.15659/ijaat.16.07.323.
- 19. Soloiu, V., Carapia, C., Smith, R., Mothershed, D. et al., "RCCI with High Reactivity S8-ULSD Blend and Low Reactivity N-Butanol," in ASME 2020 Internal Combustion Engine Division Fall Technical Conference, 2021, https://doi.org/10.1115/1.0003701v.
- Alhikami, A.F., Yao, C.-E., and Wang, W.-C., "A Study of the Spray Ignition Characteristics of Hydro-Processed Renewable Diesel, Petroleum Diesel, and Biodiesel Using a Constant Volume Combustion Chamber," Combustion and Flame 223 (2021): 55-64, https://doi.org/10.1016/j.combustflame.2020.09.033.
- 21. Santhoshkumar, A., Thangarasu, V., and Anand, R., "Performance, Combustion, and Emission Characteristics of DI Diesel Engine Using Mahua Biodiesel," *Advanced Biofuels* (2019): 291-327, https://doi.org/10.1016/b978-0-08-102791-2.00012-x.
- 22. Lobo, P., Condevaux, J., Zhenhong, Y., Kuhlmann, J. et al., "Demonstration of a Regulatory Method for Aircraft Engine

COMBUSTION CHARACTERISTICS OF LOW DCN SYNTHETIC AVIATION FUEL, IPK

- Nonvolatile PM Emissions Measurements with Conventional and ISOPARAFFINIC Kerosene Fuels," *Energy & Fuels* 30, no. 9 (2016): 7770-7777, https://doi.org/10.1021/acs.energyfuels.6b01581.
- Kang, D., Kim, D., Kalaskar, V., Violi, A. et al., "Experimental Characterization of Jet Fuels under Engine Relevant Conditions – Part 1: Effect of Chemical Composition on Autoignition of Conventional and Alternative Jet Fuels," Fuel 239 (2019): 1388-1404, https://doi.org/10.1016/j.fuel.2018.10.005.
- 24. Rothamer, D.A. and Murphy, L., "Systematic Study of Ignition Delay for Jet Fuels and Diesel Fuel in a Heavy-Duty Diesel Engine," *Proceedings of the Combustion Institute* 34, no. 2 (2013): 3021-3029, https://doi.org/10.1016/j.proci.2012.06.085.
- Soloiu, V., Weaver, A., Parker, L., Brant, A. et al., "Constant Volume Combustion Chamber (CVCC) Investigations of Aerospace F-24 and Jet-A in Low-Temperature Heat Release and Negative Temperature Coefficient Regions," *Energy Conversion and Management* 263 (2022): 115687, https://doi.org/10.1016/j.enconman.2022.115687.
- 26. Zheng, Z., Badawy, T., Henein, N., Sattler, E. et al., "Effect of Cetane Improver on Autoignition Characteristics of Low Cetane Sasol IPK Using Ignition Quality Tester (IQT)," Volume 2: Fuels; Numerical Simulation; Engine Design, Lubrication, and Applications, 2013, https://doi.org/10.1115/icef2013-19061
- 27. Wu, H., Zhen, H., Dong, X., Zhang, S. et al., "Numerical Investigation of Negative Temperature Coefficient Effects on Sooting Characteristics in a Laminar Co-Flow Diffusion Flame," *ACS Omega* 6, no. 23 (2021): 15156-15167, https://doi.org/10.1021/acsomega.1c01397.
- Szybist, J.P., Boehman, A.L., Haworth, D.C., and Koga, H., "Premixed Ignition Behavior of Alternative Diesel Fuel-Relevant Compounds in a Motored Engine Experiment," Combustion and Flame 149, no. 1-2 (2007): 112-128, https://doi.org/10.1016/j.combustflame.2006.12.011.
- Soloiu, V., Naes, T., Muinos, M., Harp, S. et al., "Comparison of Combustion and Emissions Properties of Jet-A vs. ULSD in both Indirect and Direct Compression Ignition Engines at Same IMEP," SAE Technical Paper <u>2016-01-0733</u> (2016), https://doi.org/10.4271/2016-01-0733.
- 30. Heywood, J.B., *Internal Combustion Engine Fundamentals* (New York: McGraw-Hill Education, 2018)
- Soloiu, V., Nelson, D., Covington, A., and Lewis, J., "Investigations of a Fatty Acid Methyl Ester from Poultry Fat in a Triple Vortex Separate Combustion Chamber Diesel Engine Stage One-Combustion Investigations," SAE Technical Paper 2011-01-1188 (2011), https://doi. org/10.4271/2011-01-1188.
- Soloiu, V., Moncada, J., Muinos, M., Knowles, A. et al., "Performance Evaluation - Combustion, Emissions and Vibrations-of n-Butanol Binary Mixture with ULSD in an Indirect Injection Engine," SAE Technical Paper 2017-01-0875 (2017), https://doi.org/10.4271/2017-01-0875.

- Soloiu, V., Harp, S., Watson, C., Muinos, M. et al., "Performance of an IDI Engine Fueled with Fatty Acid Methyl Esters Formulated from Cotton Seeds Oils," SAE Int. J. Fuels Lubr. 8, no. 2 (2015): 277-289, https://doi. org/10.4271/2015-01-0806.
- Soloiu, V., Gaubert, R., Muinos, M., Moncada, J. et al., "Performance of an Indirect Injected Engine Operated with ULSD#2 Blended with Fischer-Tropsch Synthetic Kerosene," SAE Technical Paper 2017-01-1283 (2017), https://doi. org/10.4271/2017-01-1283.
- Dunn, R.O., "Fuel Properties of Biodiesel/Ultra-Low Sulfur Diesel (ULSD) Blends," *Journal of the American Oil* Chemists' Society 88, no. 12 (2011): 1977-1987, https://doi.org/10.1007/s11746-011-1871-3.
- 36. Flora, G., Kosir, S.T., Behnke, L., Stachler, R.D. et al., "Properties Calculator and Optimization for Drop-in Alternative Jet Fuel Blends," in *AIAA Scitech 2019 Forum*, 2019, https://doi.org/10.2514/6.2019-2368.
- 37. Joshi, U., Zheng, Z., Shrestha, A., Henein, N. et al., "An Investigation on Sensitivity of Ignition Delay and Activation Energy in Diesel Combustion," Volume 1: Large Bore Engines; Fuels; Advanced Combustion; Emissions Control Systems, 2014, https://doi.org/10.1115/icef2014-5587.
- Jürgens, S., Oßwald, P., Selinsek, M., Piermartini, P. et al., "Assessment of Combustion Properties of Non-Hydroprocessed Fischer-Tropsch Fuels for Aviation," Fuel Processing Technology 193 (2019): 232-243, https://doi. org/10.1016/j.fuproc.2019.05.015.
- 39. Hui, X., Kumar, K., Sung, C.-J., Edwards, T. et al., "Experimental Studies on the Combustion Characteristics of Alternative Jet Fuels," *Fuel* 98 (2012): 176-182, https://doi.org/10.1016/j.fuel.2012.03.040.
- 40. Burden, S., Tekawade, A., and Oehlschlaeger, M.A., "Ignition Delay Times for Jet and Diesel Fuels: Constant Volume Spray and Gas-Phase Shock Tube Measurements," *Fuel* 219 (2018): 312-319, https://doi.org/10.1016/j.fuel.2018.01.113.
- 41. Allen, C., Valco, D., Toulson, E., Edwards, T. et al., "Ignition Behavior and Surrogate Modeling of JP-8 and of Camelina and Tallow Hydrotreated Renewable Jet Fuels at Low Temperatures," *Combustion and Flame* 160, no. 2 (2013): 232-239, https://doi.org/10.1016/j.combustflame.2012.10.008.
- 42. Eng, J.A., "Characterization of Pressure Waves in Hcci Combustion," SAE Technical Paper <u>2002-01-2859</u> (2002), https://doi.org/10.4271/2002-01-2859.
- 43. George, R.M., Badawy, T., and Henein, N., "Experimental Study for the Effect of Fuel Properties on the Ion Current, Combustion, and Emission in a High-Speed Diesel Engine," SAE Technical Paper 2014-01-1263 (2014), https://doi.org/10.4271/2014-01-1263.
- 44. Zheng, Z., Joshi, U., Henein, N., and Sattler, E., "Effect of Cetane Improver on Combustion and Emission Characteristics of Coal-Derived Sasol IPK in a Single Cylinder Diesel Engine," Volume 1: Large Bore Engines; Fuels; Advanced Combustion; Emissions Control Systems, 2014, https://doi.org/10.1115/icef2014-5589.

Contact Information

Dr. Valentin Soloiu, Professor

Director of Automotive and Aerospace Combustion Laboratories Georgia Southern University, USA vsoloiu@georgiasouthern.edu

Acknowledgments

We would like to acknowledge the Air Force Research Laboratories for supplying the fuel, Samuel Oleski from Kistler, Lucius Miller from AVL, Michael Rankin from PACLP, Coty Harrison from Yokogawa, and the support of the National Science Foundation under Grant no. 1950207.

Definitions/Abbreviations

AFR - Air Fuel Ratio

AHRR - Apparent Heat Release

ATDC - After Top Dead Center

BTDC - Before Top Dead Center

BMEP - Break Mean Effective Pressure

CAD - Crank Angle Degree

CA10 - Crank Angle Degree @ 10% mass burned

CA50 - Crank Angle Degree @ 50% mass burned

CA90 - Crank Angle Degree @ 90% mass burned

CRDI - Common Rail Direct Injection

CD - Combustion Delay

CDC - Conventional Diesel Combustion

CI - Compression Ignition

CN - Cetane Number

CO - Carbon Monoxide

CTL - Coal-to-Liquid

CVCC - Constant Volume Combustion Chamber

D - Engine Bore

DCN - Derived Cetane Number

DI - Direct Injection

Dv10 - Largest Droplet Size of 10% of Fuel Spray

Dv50 - Largest Droplet Size of 50% of Fuel Spray

Dv90 - Largest Droplet Size of 90% of Fuel Spray

DTA - Differential Thermal Analysis

EPA - Environmental Protection Agency

FT - Fischer-Tropsch

FTIR - Fourier Transform Spectroscopy

HC - Hydrocarbons

HHV - Higher Heating Value

HTHR - High Temperature Heat Release

ID - Ignition Delay

IDI - Indirect Injection

IMEP - Indicated Mean Effective Pressure

IPK - Iso-Paraffinic Kerosene

LHV - Lower Heating Value

LTC - Low Temperature Combustion

LTHR - Low Temperature Heat Release

MC - Main Chamber

N - Engine Speed

NTCR - Negative Temperature Coefficient Region

NOx - Nitrogen oxides

PC - Pre-chamber

POI - Point of Inflection

PRR - Pressure Rise Rate

PPRR - Peak Pressure Rise Rate

Re - Reynolds Number

RPM - Revolutions Per Minute

RI - Ringing Intensity

S - Stroke

SAF - Sustainable Aviation Fuel

SMD - Sauter Mean Diameter

TA10 - Temperature @ 10% mass vaporized

TA50 - Temperature @ 50% mass vaporized

TA90 - Temperature @ 90% mass vaporized

TGA - Thermogravimetric Analysis

UHC - Unburnt Hydrocarbons

ULSD - Ultra-Low Sulfur Diesel

^{© 2023} SAE International. All rights reserved. No part of this publication may be reproduced, stored in a retrieval system, or transmitted, in any form or by any means, electronic, mechanical, photocopying, recording, or otherwise, without the prior written permission of SAE International.